

Electronic structure of Li_2O_2 {0001} surfaces

Maxwell D. Radin · Feng Tian · Donald J. Siegel

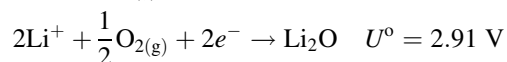
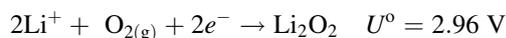
Received: 17 February 2012 / Accepted: 3 May 2012 / Published online: 26 May 2012
© Springer Science+Business Media, LLC 2012

Abstract The surface properties of the Li_2O_2 discharge phase are expected to impact strongly the capacity, rate capability, and rechargeability of Li-oxygen batteries. Prior calculations have suggested that the presence of half-metallic surface states in Li_2O_2 may mitigate electrical passivation resulting from the growth of Li_2O_2 , which is a bulk insulator. Here we revisit the electronic structure of bulk Li_2O_2 and the dominant Li_2O_2 {0001} surface by comparing results obtained with the PBE GGA functional, the HSE06 hybrid functional, and quasiparticle GW methods. Our results suggest that the bulk band gap lies between the value predicted by the G_0W_0 method, 5.15 eV, and the value predicted by the self-consistent quasiparticle GW (scGW) approximation, 6.37 eV. The PBE, HSE06, and scGW methods agree that the most stable surface, an oxygen-rich {0001} termination, is indeed half-metallic. This result supports the notion that the electronic structure of surfaces may play an important role in understanding performance limitations in Li-oxygen batteries.

Introduction

Energy storage plays a key role in many emerging technologies. Prominent examples include battery-powered electric vehicles and the storage of intermittent, renewable power sources on the electrical grid. State-of-the-art rechargeable Li-ion batteries are costly and exhibit specific energy densities of ~ 120 Wh/kg (system level) [1], which is inadequate for many applications. Among alternative candidates for high-density energy storage, the Li-oxygen battery [2, 3] (Fig. 1) has a theoretical specific energy ten times higher than that of current Li-ion battery chemistries [1, 4, 5]. The practical specific energy has been recently estimated to be 1400–1800 Wh/kg (cell level), depending on whether the mass of oxygen is included [2].

In the absence of solvent decomposition [6–10] the discharge of a Li- O_2 battery can potentially occur via two electrochemical reactions resulting in the formation of insoluble lithium peroxide (Li_2O_2) or lithium oxide (Li_2O) [11]:



Abraham and Jiang [12] were the first to demonstrate a rechargeable Li-oxygen battery; their prototype consisted of a lithium metal anode, an air-breathing carbon cathode, and a Li^+ conductive polymer electrolyte membrane. Based on Raman spectra the discharge product was identified as Li_2O_2 [12], a result which has been confirmed by subsequent experiments [6, 13–16]. On the other hand, while the formation of Li_2O has also been suggested by several authors [15, 17–20], definitive evidence for its formation is rare [20]. The decomposition of Li_2O_2 to Li and O_2 during recharge has been confirmed, which indicates the formation of Li_2O_2 is electrochemically reversible [6, 16, 21].

M. D. Radin
Department of Physics, University of Michigan, Ann Arbor,
MI 48109-2125, USA

F. Tian · D. J. Siegel
Department of Mechanical Engineering, University of Michigan,
Ann Arbor, MI 48109-2125, USA

D. J. Siegel
Applied Physics Program, University of Michigan, Ann Arbor,
MI 48109-2125, USA

D. J. Siegel (✉)
Michigan Energy Institute, University of Michigan, Ann Arbor,
MI 48109-2125, USA
e-mail: djsiegel@umich.edu

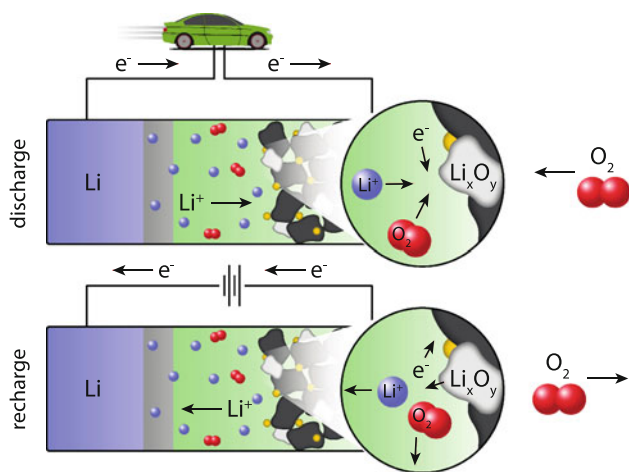


Fig. 1 Schematic for a Li–oxygen cell during discharge and recharge. During discharge, Li ions (blue) pass through the separator/solid electrolyte (gray) and electrolyte (green) to react with dissolved oxygen (red) and electrons in the cathode. A lithium oxide phase (gray) forms on top of the carbon support (black) and, possibly, a catalyst (gold). During recharge, the reaction is reversed and O₂ is released (Color figure online)

Given that Li₂O₂ is expected to be a bulk insulator, electrical passivation via growth of a resistive discharge product has been proposed as a possible performance limitation [22]. Macro-scale models have indicated that an insulating discharge product can severely limit discharge capacity [22], and electron transport simulations combined with flat electrode experiments based on an outer sphere redox couple have suggested that a 5–10 nm layer of monocrystalline Li₂O₂ results in complete electrical passivation of the electrode [23]. However, the discharge product in a practical cell is likely not a monolithic film; vacancies, surfaces, grain boundaries, or other imperfections may provide conduction mechanisms that mitigate passivation [2, 22]. Indeed, it would be difficult to explain the observed size of Li₂O₂ particles (~350 nm) [14] without introducing such a conduction pathway. In this paper, we focus on the possibility of conduction through Li₂O₂ surface states. Motivation for this work comes from an earlier report by Hummelshøj et al. [24] who showed that lithium vacancies might yield conductivity in bulk Li₂O₂. This suggests that other defects such as grain boundaries or surfaces, particularly those that are Li-deficient/O-rich, could also play a role in electron transport. The goal of this study is to use a variety of electronic structure methods to carefully examine the electronic structure of the O-rich Li₂O₂ {0001} surface, which we identified as being the most stable Li₂O₂ surface in a prior study [25]. Although other types of imperfections such as point defects may impact charge transport properties, in this study we focus on the role of surfaces; we will report on the role played by other defect types in a subsequent publication.

The modeling of charge transport in bulk Li₂O₂ [24, 26–28] and across Li₂O₂ interfaces [23, 29] is an active area of research. For example, recent calculations have explored the formation of small hole [26] and electron [27] polarons in Li₂O₂, with one study reporting a low barrier for hole polaron migration, which could potentially allow for *p*-type conductivity [26]. These results indicate that additional study is needed to resolve the competition between band conduction [24] and polaronic [26, 27] conduction in bulk Li₂O₂.

Regarding surfaces, a small number of studies have used first-principles calculations to examine the surfaces of Li-oxygen discharge phases [24, 25, 30, 31]. Seriani [30] performed the first calculations of formation energies for Li₂O₂ and Li₂O surfaces, while Mo et al. [31] and Hummelshøj et al. [24] have studied adsorption and desorption pathways on Li₂O₂ surfaces.

In a recent study [25], we used density functional theory calculations to identify stable surfaces in Li₂O₂ and Li₂O from a pool of 40 candidate surfaces. Combining the calculated energies with the Wulff construction [32], we found that Li₂O₂ crystallites exhibit two low-energy facets: an oxygen-rich {0001} termination which comprises a majority of the crystallite surface area, and an oxygen-rich {1 $\bar{1}$ 00} surface making up the remainder. The free energies for these surfaces are summarized in Table 1. Given that the difference in formation energies between the {1 $\bar{1}$ 00} and {11 $\bar{2}$ 0} surfaces (i.e., 7 meV/atom) is comparable to typical uncertainties in the calculation, it is likely that the {11 $\bar{2}$ 0} surface will also contribute to the crystallite surface area. For example, Fig. 2 shows a revised Wulff plot in which the {1 $\bar{1}$ 00} and {11 $\bar{2}$ 0} surfaces are assigned equal formation energies of 23 meV/Å². Compared to the morphology predicted in Ref. [25], the revised Wulff plot yields Li₂O₂ crystallites having a lower aspect ratio and a more platelet-like appearance. Scanning electron microscopy experiments on discharged Li-oxygen cells have also observed platelet-shaped particles, but with a toroid-like morphology [14].

An examination of the electronic structure of the stable Li₂O₂ surfaces indicated that they were magnetic and half-metallic [25], i.e., conducting in one spin channel and

Table 1 Calculated free energies of low-energy Li₂O₂ surfaces at 300 K and P(O₂) = 1 atm as reported in Ref. [25]

Surface index	Surface free energy, γ (meV/Å ²)	Surface free energy, γ (meV/atom)
{0001}	6	26
{1 $\bar{1}$ 00}	21	73–85
{11 $\bar{2}$ 0}	26	80–187

The corresponding surface structures are shown in Fig. 3. The free energy per surface atom is determined by dividing the formation energy per unit cell by the number of surface sites. In cases where the number of surface sites is ambiguous, a range of values is provided

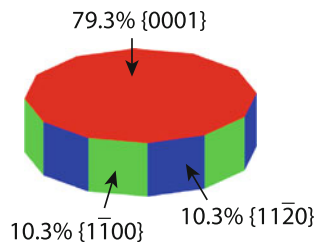


Fig. 2 Wulff construction illustrating the equilibrium crystallite shape for Li_2O_2 particles assuming the $\{1\bar{1}00\}$ and $\{11\bar{2}0\}$ surfaces have equal formation energies of $23 \text{ meV}/\text{\AA}^2$ (Color figure online)

insulating in the other. Based on these findings it was suggested [25] that half-metallic surface states could mitigate the electrical passivation expected to result from the growth of Li_2O_2 (which is a bulk insulator) during discharge [2, 22]. It was also noted [25] that the presence of conducting surfaces in Li_2O_2 —and the absence of the same in Li_2O —correlates with the differing electrochemical reactivity of these phases, suggesting that surface effects may at least partially account for the fact that Li_2O_2 can be electrochemically decomposed [6, 16, 21, 33] whereas Li_2O is electrochemically inactive [33–35].

As density functional theory (DFT) is strictly a ground state theory, it is well known that conventional local and gradient-corrected density functionals generally under-predict band gaps [36]. DFT also incorrectly predicts many materials, including some wide-gap transition metal insulators [37] and narrow-gap non-transition metal semiconductors [36, 38, 39], to be semi-metals or conductors. Given the uncertainty associated with band gap predictions within DFT, in our previous study of Li_2O_2 surface states we also performed calculations on the most stable surface using the HSE06 hybrid functional [40, 41] (the HSE06 functional is known to provide better estimates of band gaps due to its partial incorporation of exact exchange) [41, 42]. In this study we revisit the electronic structure of bulk Li_2O_2 as well as that of the most stable surface, shown in Fig. 3a, by comparing results obtained with the PBE GGA functional [43], the HSE06 hybrid functional [40, 41], and GW techniques [44, 45].

Our calculations find that the bulk band gaps for Li_2O_2 predicted by PBE, HSE06, G_0W_0 , and scGW are 1.99,

4.19, 5.15, and 6.37 eV, respectively. Based on prior studies comparing G_0W_0 and scGW to experiments [38, 44], we expect that the true band gap lies between the latter two values. We find that PBE, HSE06, and scGW all agree that the $\{0001\}$ surface is indeed half-metallic. These results are consistent with our prior hypothesis that surface conductivity may play an important role in the electrical passivation and electrochemical reversibility of Li_2O_2 . As these results neglect effects arising from an electrolyte/solvent, additional study is needed to examine the impact of the liquid solvent/ Li_2O_2 junction on surface electronic structure. Experimental characterization of Li_2O_2 surface phenomena is called for.

Computational methods

First-principles calculations were performed using four techniques implemented in the Vienna Ab initio Simulation Package (VASP) [46–49]: (i) the Perdew–Burke–Ernzerhof (PBE) generalized gradient approximation (GGA) [43], (ii) the Heyd–Scuseria–Ernzerhof (HSE06) hybrid functional [40, 41], (iii) the non-self-consistent G_0W_0 method [45], and (iv) the self-consistent quasiparticle GW approximation (scGW) [44]. A PBE calculation was used as the starting point for all G_0W_0 and scGW calculations. The rigorous treatment of excited states provided by the scGW method is intended to validate the surface electronic structure predicted by the more approximate PBE and (to a lesser extent) HSE06 methods, although due to the computational expense of this approach, our scGW calculations are restricted to smaller supercells and fewer k-points for surface slabs. The most common GW approximation (GWA) technique, referred to as the G_0W_0 method, is a non-self-consistent technique in that it applies the GWA as a perturbation to the DFT wavefunctions and one-electron energies [44]. One limitation of the G_0W_0 method, which is common to all non- and partially self-consistent GWA methods, is that it is sensitive to the wavefunctions and one-electron energies used as the starting point for the quasiparticle calculation [38]. For example, in the case of

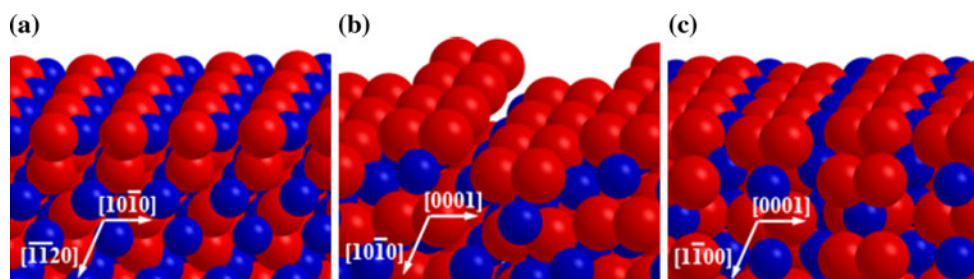


Fig. 3 Structures of the lowest energy **a** $\{0001\}$, **b** $\{1\bar{1}00\}$, and **c** $\{11\bar{2}0\}$ Li_2O_2 surfaces as reported in Ref. [25]. Large red spheres and small blue spheres represent O and Li atoms, respectively. All surfaces were found to be oxygen-rich (Color figure online)

InN, LDA + G_0W_0 has been found to predict no band gap whereas HSE + G_0W_0 correctly predicts the existence of a gap [39]. We therefore, also employ the scGW method because the wavefunctions are determined in a self-consistent manner; therefore, the results are not sensitive to the starting point of the calculation.

Projector-augmented wave (PAW) potentials [50, 51] were employed with valence states of $2s$ for Li and $2s2p$ for O. A cutoff energy of 400 eV was used for the plane wave basis, in conjunction with the Monkhorst–Pack scheme [52] for k-point sampling. Surface calculations were spin-polarized, whereas bulk Li_2O_2 is known to be non-magnetic. Electronic occupancies were determined by the tetrahedron method [53] for self-consistent GGA calculations not involving geometry optimization; a Gaussian smearing of width 0.2 eV was used for all other cases. For structural optimizations, all ions were relaxed using the PBE functional to a force tolerance of 0.02 eV/Å or less.

Surface calculations were performed on symmetric slabs within a supercell containing a ~ 10 Å vacuum region. The length of the supercell (including the vacuum region) for PBE and HSE06 calculations on the {0001} surface was 50.0 Å. This cell was comprised of 43 atoms, which formed 11 oxygen dimer layers. Due to computational constraints, a smaller supercell (19.3 Å, 11 atoms) was used for G_0W_0 and scGW calculations. The k-point grid for self-consistent calculations was $5 \times 5 \times 1$; denser grids ($11 \times 11 \times 1$) were used for the PBE and HSE06 density of states (DOS) calculations. The bulk DOS was calculated on a single unit cell with a $7 \times 7 \times 3$ k-point grid. The reported band gaps were calculated as the difference between the eigenvalues of the highest occupied state and the lowest unoccupied state. As the band gaps predicted by GWA methods are sensitive to the number of bands used in the calculation, we have verified that the bulk band gaps are converged to within 0.02 eV with respect to the number of bands.

Bulk properties

Figure 4 shows the DOS for bulk Li_2O_2 calculated using the PBE GGA, HSE06, G_0W_0 , and scGW methods. The band gaps predicted by these four methods are 1.99, 4.19, 5.15, and 6.37 eV (the apparent gaps in Fig. 4 are ~ 0.4 eV smaller due to the broadening of the energy levels associated with the Gaussian smearing). Table 2 summarizes the predicted band gaps alongside comparable calculations from the literature. Our PBE result is close to the band gap predicted by other DFT calculations, but is much smaller than the band gaps predicted by hybrid functionals such as HSE06. This is consistent with the fact that HSE06 is known to offer significantly improved band gaps compared GGA [41, 42], although it tends to underestimate band gaps in

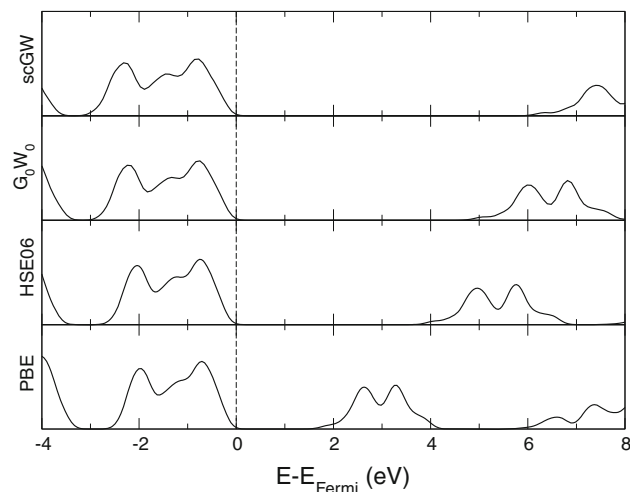


Fig. 4 Density of states (in arbitrary units) for bulk Li_2O_2 calculated using four different methods: (from bottom to top) PBE, HSE06, G_0W_0 , and scGW

Table 2 Calculated band gaps for Li_2O_2 in eV, organized by calculation method

Method type	This work	Prior work
DFT	1.99 (PBE)	1.98 (LDA) [54]
		1.88 (RPBE) [24]
		1.94 (PBE) [28]
Hybrid functional	4.19 (HSE)	4.2 (HSE) [26]
		4.5 (HSE) [27]
		4.44 (B3LYP) [55]
GWA	6.37 (scGW) 5.15 (G_0W_0)	4.91 (G_0W_0) [24]
		4.81 (G_0W_0) [28]

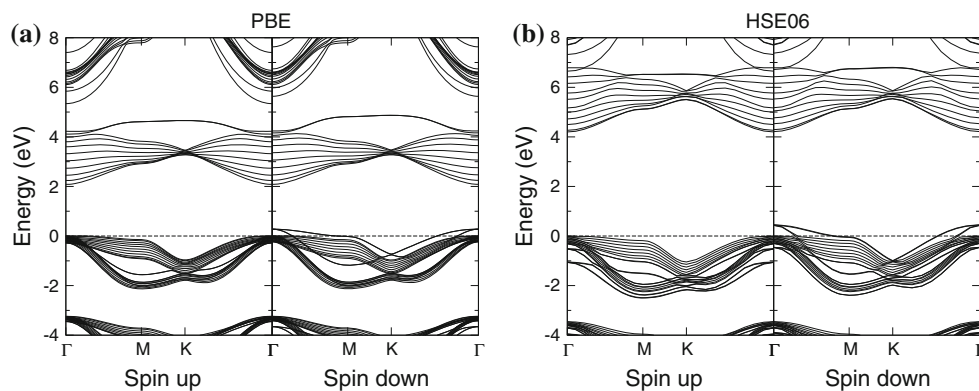
A GGA calculation was used as the starting point for all GWA calculations shown above

wide-gap insulators [56]. The results of our G_0W_0 calculation also agree with previously reported GGA + G_0W_0 calculations. GGA + G_0W_0 are known to systematically underestimate band gaps; in some cases, such as ZnO, the gap can be underestimated by as much as 30 % [38]. On the other hand, the band gap we find from the scGW method is notably larger. Indeed, the scGW method is known to consistently overestimate band gaps, often by 10–15 % [44]. Therefore, the values found from G_0W_0 and scGW, 5.15 and 6.37 eV, likely represent lower and upper bounds on the true band gap. To the best of our knowledge, no experimental value has been reported for the band gap of Li_2O_2 .

{0001} Surface

Figure 5 shows the band structure of the {0001} surface as predicted by the PBE GGA and HSE06 functionals. Qualitatively, both functionals are in agreement: this

Fig. 5 Surface band structure for the most stable Li_2O_2 {0001} surface calculated using **a** the PBE GGA functional and **b** the HSE06 hybrid functional. The horizontal dashed line represents the Fermi level. Spin-up and spin-down bands are shown in the left and right panels, respectively



surface is insulating in the majority (spin-up) channel and conducting in the minority (spin-down) channel. However, we note a few quantitative differences between the two band structures. First, HSE06 yields a larger band gap (4.20 eV in the spin-up channel) than PBE (2.09 eV). These values are comparable to the bulk band gaps discussed above. Secondly, the bandwidth of the metallic surface states is somewhat larger in the HSE06 calculation than in the PBE calculation (2.00 eV vs. 1.46 eV). This is also consistent with past studies, which have shown that HSE06 often yields larger bandwidths in metals [56].

Figure 6 shows the layer-projected density of states and magnetization density from PBE, HSE06, and scGW calculations, which highlights the localization of the conductive states near the surface. A visual inspection of the

band-decomposed charge density (not shown) indicates that the surface states are formed by oxygen π^* orbitals, which resemble a torus lying in a plane parallel to the surface. The two surface bands seen crossing the Fermi level are both very nearly doubly degenerate, corresponding to the two surfaces of the slab. (The splitting is too small to be visible in Fig. 5). The smallness of the splitting indicates that the slab is sufficiently thick that the coupling between the surfaces is negligible.

The calculations performed using PBE, HSE06, and scGW confirm our prior result that the {0001} surface is half-metallic. The origin of this behavior can be understood in terms of electrostatic considerations, which often control the structural and electronic properties of surfaces [57, 58]. Figure 7 shows the {0001} slab used in our scGW

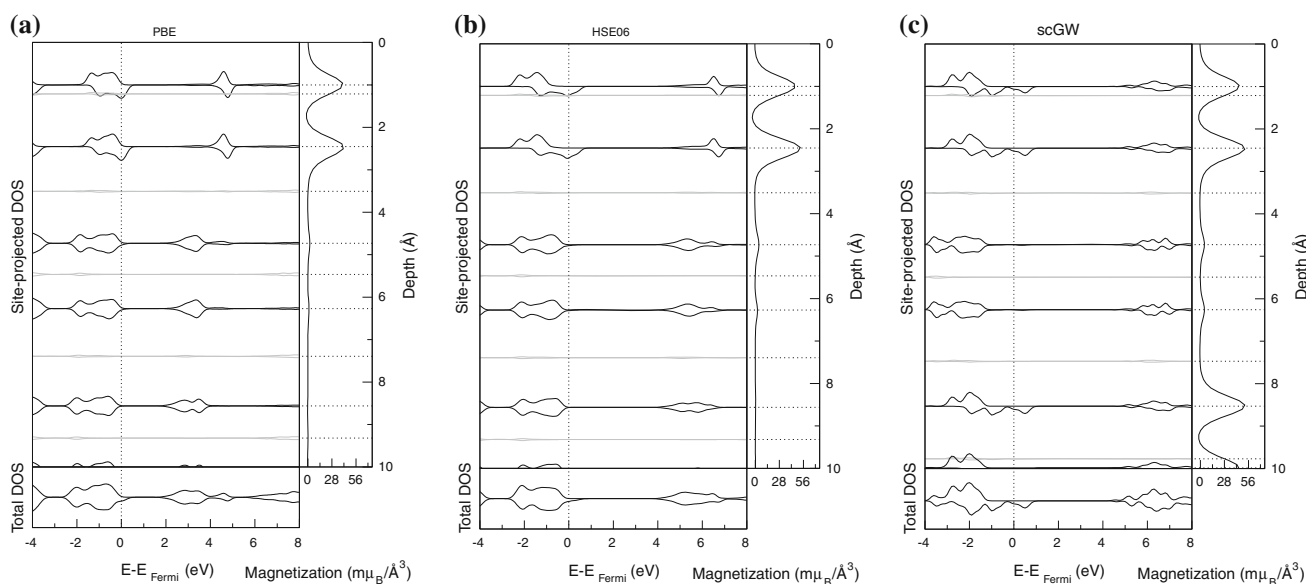


Fig. 6 Calculated layer-projected spin density of states and planar-averaged magnetization for the lowest energy {0001} surface using the **a** PBE GGA, **b** HSE06, and **c** GGA + scGW methods. The positions of the DOS traces are staggered vertically to reflect the relative spacing of the atomic layers. Black traces are for oxygen layers, and gray traces are for lithium layers. In the magnetization density plots horizontal dotted lines indicate the positions of the

atomic planes. Surface atoms appear at the top of each plot, and subsurface atoms (etc.) are located successively below. The bottom panel plots the total DOS for the entire slab. As a smaller slab consisting of six oxygen layers was used in the scGW calculation (c), the DOS for all six of these layers is visible. The magnetization at a depth of 8–10 Å in panel c is due to the surface O sites on the bottom of the slab

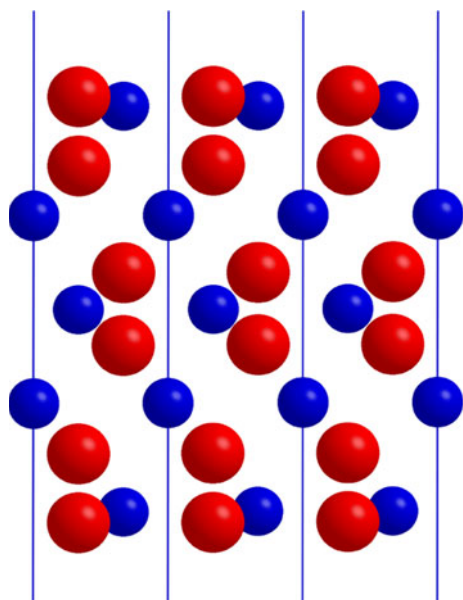


Fig. 7 Three unit cells of a relaxed {0001} slab. *Large red spheres* represent oxygen atoms, and *small blue spheres* represent lithium atoms. The *solid lines* indicate the cell boundaries (Color figure online)

calculations, which consists of alternating layers of Li and O atoms with each layer containing one atom per unit cell. Because of the polar nature of this surface, a compensating charge of $+1/2e$ per unit cell is required for electrostatic stability; this is achieved by the partial depletion of oxygen $2p$ states near the surface. The presence of a fractional charge on the surface requires that at least one band is partially filled (from Fig. 5 we see that there are in fact two distinct bands with partial occupancy; this is due to the twofold degeneracy of the π^* orbitals at the top of the valence band). The surface conductivity of the stable Li-deficient {0001} surface and bulk conductivity induced by lithium vacancies [24] appear to be analogous; in both cases, the deficiency of lithium and subsequent depletion of oxygen $2p$ states results in partially filled bands.

The recent prediction of hole polaron formation in bulk Li_2O_2 [26] suggests that the free holes created by cleaving the O-rich {0001} surface may potentially localize to form surface polarons. Indeed, our preliminary calculations indicate that this is the case. Although such carrier localization could preclude band conduction, facile surface polaron hopping may also provide an important pathway for charge transport along Li_2O_2 surfaces. As prior calculations have indicated that the energy barrier for hole polaron migration within the {0001} plane of bulk Li_2O_2 is less than 68 meV [26], we expect {0001} surface polarons to be quite mobile. Surface polaron formation and migration will be addressed in greater detail in a forthcoming publication.

We note that in an actual Li-oxygen cell the discharge product will be interfaced with a liquid solvent (including

an electrolyte), an effect which is omitted in this study. Therefore, further work is needed to determine if solvent adsorption could alter the electronic structure of this surface. Finally, we note that the presence of conductive surface states suggests that grain boundaries in Li_2O_2 may also be conductive; this possibility will be addressed in a future study.

Conclusion

Calculations have been performed to analyze the electronic structure of bulk Li_2O_2 and its most stable surface using the PBE GGA functional, the HSE06 hybrid functional, and GW methods. The bulk band gaps predicted by PBE, HSE06, G_0W_0 , and scGW are 1.99, 4.19, 5.15, and 6.37 eV, respectively. Based on prior comparisons between these methods and experiments, we expect the actual band gap to lie between 5.15 and 6.37 eV. The globally most stable surface, an oxygen-rich {0001} surface, is found to be half-metallic by PBE, HSE06, and scGW calculations. The conducting nature of this surface can be described in terms of band-filling considerations. Our discovery of conducting surfaces supports the hypothesis that surface conductivity mitigates electrical passivation and might also account for the different electrochemical reversibilities of Li_2O_2 and Li_2O formation. Experimental characterization of Li_2O_2 surfaces is called for. Likewise further theoretical work is required to understand the electronic structure of other low-energy Li_2O_2 surfaces, and the possible role of surface polarons and solvent adsorption on surface properties.

Acknowledgements Financial support was provided by the U.S. Department of Energy's U.S.-China Clean Energy Research Center for Clean Vehicle Consortium, Grant DE-PI0000012 and the University of Michigan-Shanghai Jiao Tong University Collaboration on Renewable Energy Science and Technology.

References

1. Cairns EJ, Albertus P (2010) *Annu Rev Chem Biomol Eng* 1(1):299
2. Christensen J, Albertus P, Sanchez-Carrera RS, Lohmann T, Kozinsky B, Liedtke R, Ahmed J, Kojic A (2012) *J Electrochem Soc* 159(2):R1
3. Bruce PG, Freunberger SA, Hardwick LJ, Tarascon J-M (2012) *Nat Mater* 11(1):19
4. Beattie SD, Manolescu DM, Blair SL (2009) *J Electrochem Soc* 156(1):A44. doi:10.1149/1.3005989
5. Girishkumar G, McCloskey B, Luntz AC, Swanson S, Wilcke W (2010) *J Phys Chem Lett* 1(14):2193. doi:10.1021/jz1005384
6. McCloskey BD, Bethune DS, Shelby RM, Girishkumar G, Luntz AC (2011) *J Phys Chem Lett* 2(10):1161. doi:10.1021/jz200352v
7. Freunberger SA, Chen YH, Peng ZQ, Griffin JM, Hardwick LJ, Barde F, Novak P, Bruce PG (2011) *J Am Chem Soc* 133(20):8040. doi:10.1021/ja2021747

8. Xiao J, Hu JZ, Wang DY, Hu DH, Xu W, Graff GL, Nie ZM, Liu J, Zhang JG (2011) *J Power Sources* 196(13):5674. doi:[10.1016/j.jpowsour.2011.02.060](https://doi.org/10.1016/j.jpowsour.2011.02.060)
9. Xu W, Viswanathan VV, Wang DY, Towne SA, Xiao J, Nie ZM, Hu DH, Zhang JG (2011) *J Power Sources* 196(8):3894. doi:[10.1016/j.jpowsour.2010.12.065](https://doi.org/10.1016/j.jpowsour.2010.12.065)
10. Mizuno F, Nakanishi S, Kotani Y, Yokoishi S, Iba H (2010) *Electrochemistry* 78(5):403
11. Chase MW (1998) NIST-JANAF thermochemical tables. American Institute of Physics, Woodbury
12. Abraham KM, Jiang Z (1996) *J Electrochem Soc* 143(1):1
13. Débart A, Bao J, Armstrong G, Bruce PG (2007) *J Power Sources* 174(2):1177. doi:[10.1016/j.jpowsour.2007.06.180](https://doi.org/10.1016/j.jpowsour.2007.06.180)
14. Lu YC, Kwabi DG, Yao KPC, Harding JR, Zhou JG, Zuin L, Shao-Horn Y (2011) *Energy Environ Sci* 4(8):2999. doi:[10.1039/c1ee01500a](https://doi.org/10.1039/c1ee01500a)
15. Laoire CO, Mukerjee S, Plichta EJ, Hendrickson MA, Abraham KM (2011) *J Electrochem Soc* 158(3):A302. doi:[10.1149/1.3531981](https://doi.org/10.1149/1.3531981)
16. Ogasawara T, Débart A, Holzapfel M, Novak P, Bruce PG (2006) *J Am Chem Soc* 128(4):1390. doi:[10.1021/ja056811q](https://doi.org/10.1021/ja056811q)
17. Read J (2002) *J Electrochem Soc* 149(9):A1190. doi:[10.1149/1.1498256](https://doi.org/10.1149/1.1498256)
18. Thapa AK, Saimen K, Ishihara T (2010) *Electrochem Solid State Lett* 13(11):A165. doi:[10.1149/1.3481762](https://doi.org/10.1149/1.3481762)
19. Zhang SS, Foster D, Read J (2010) *J Power Sources* 195(4):1235. doi:[10.1016/j.jpowsour.2009.08.088](https://doi.org/10.1016/j.jpowsour.2009.08.088)
20. Thapa AK, Ishihara T (2011) *J Power Sources* 196(16):7016. doi:[10.1016/j.jpowsour.2010.09.112](https://doi.org/10.1016/j.jpowsour.2010.09.112)
21. Lu YC, Gasteiger HA, Parent MC, Chiloyan V, Shao-Horn Y (2010) *Electrochem Solid State Lett* 13(6):A69. doi:[10.1149/1.3363047](https://doi.org/10.1149/1.3363047)
22. Albertus P, Girishkumar G, McCloskey B, Sanchez-Carrera RS, Kozinsky B, Christensen J, Luntz AC (2011) *J Electrochem Soc* 158(3):A343. doi:[10.1149/1.3527055](https://doi.org/10.1149/1.3527055)
23. Viswanathan V, Thygesen KS, Hummelshøj JS, Nørskov JK, Girishkumar G, McCloskey BD, Luntz AC (2011) *J Chem Phys* 135(21):214704
24. Hummelshøj JS, Blomqvist J, Datta S, Vegge T, Rossmeisl J, Thygesen KS, Luntz AC, Jacobsen KW, Nørskov JK (2010) *J Chem Phys* 132(7):071101. doi:[10.1063/1.3298994](https://doi.org/10.1063/1.3298994)
25. Radin MD, Rodriguez JF, Tian F, Siegel DJ (2011) *J Am Chem Soc* 134(2):1093. doi:[10.1021/ja208944x](https://doi.org/10.1021/ja208944x)
26. Ong SP, Mo Y, Ceder G (2012) *Phys Rev B* 85(8):081105
27. Kang J, Jung YS, Wei S-H, Dillon AC (2012) *Phys Rev B* 85(3):035210
28. Garcia-Lastra JM, Bass JD, Thygesen KS (2011) *J Chem Phys* 135(12):121101
29. Chen JZ, Hummelshøj JS, Thygesen KS, Myrdal JSG, Nørskov JK, Vegge T (2011) *Catal Today* 165(1):2. doi:[10.1016/j.cattod.2010.12.022](https://doi.org/10.1016/j.cattod.2010.12.022)
30. Seriani N (2009) *Nanotechnology* 20(44):445703. doi:[10.1088/0957-4484/20/44/445703](https://doi.org/10.1088/0957-4484/20/44/445703)
31. Mo Y, Ong SP, Ceder G (2011) *Phys Rev B* 84(20):205446
32. Wulff G (1901) *Z Krystallogr Miner* 34(5/6):449
33. Xu W, Xu K, Viswanathan VV, Towne SA, Hardy JS, Xiao J, Nie Z, Hu D, Wang D, Zhang J-G (2011) *J Power Sources* 196(22):9631. doi:[10.1016/j.jpowsour.2011.06.099](https://doi.org/10.1016/j.jpowsour.2011.06.099)
34. Obrovac MN, Dunlap RA, Sanderson RJ, Dahn JR (2001) *J Electrochem Soc* 148(6):A576
35. Poizot PL, Grugeon S, Dupont L, Tarascon J-M (2000) *Nature* 407:496
36. Martin RM (2004) *Electronic structure: basic theory and practical methods*. Cambridge University Press, Cambridge
37. Cococcioni M, de Gironcoli S (2005) *Phys Rev B* 71(3):035105. doi:[10.1103/PhysRevB.71.035105](https://doi.org/10.1103/PhysRevB.71.035105)
38. Shishkin M, Kresse G (2007) *Phys Rev B* 75(23):235102
39. Fuchs F, Furthmüller J, Bechstedt F, Shishkin M, Kresse G (2007) *Phys Rev B* 76(11):115109
40. Heyd J, Scuseria GE, Ernzerhof M (2003) *J Chem Phys* 118(18):8207. doi:[10.1063/1.1564060](https://doi.org/10.1063/1.1564060)
41. Krukau AV, Vydrov OA, Izmaylov AF, Scuseria GE (2006) *J Chem Phys*. doi:[10.1063/1.2404663](https://doi.org/10.1063/1.2404663)
42. Henderson TM, Paier J, Scuseria GE (2011) *Phys Status Solidi B* 248(4):767. doi:[10.1002/pssb.201046303](https://doi.org/10.1002/pssb.201046303)
43. Perdew JP, Burke K, Ernzerhof M (1996) *Phys Rev Lett* 77(18):3865
44. Shishkin M, Marsman M, Kresse G (2007) *Phys Rev Lett* 99(24):246403
45. Shishkin M, Kresse G (2006) *Phys Rev B* 74(3):035101
46. Kresse G, Furthmüller J (1996) *Comput Mater Sci* 6(1):15
47. Kresse G, Furthmüller J (1996) *Phys Rev B* 54(16):11169
48. Kresse G, Hafner J (1993) *Phys Rev B* 47(1):558
49. Kresse G, Hafner J (1994) *Phys Rev B* 49(20):14251
50. Blöchl PE (1994) *Phys Rev B* 50(24):17953. doi:[10.1103/PhysRevB.50.17953](https://doi.org/10.1103/PhysRevB.50.17953)
51. Kresse G, Joubert D (1999) *Phys Rev B* 59(3):1758. doi:[10.1103/PhysRevB.59.1758](https://doi.org/10.1103/PhysRevB.59.1758)
52. Monkhorst HJ, Pack JD (1976) *Phys Rev B* 13(12):5188
53. Blöchl PE, Jepsen O, Andersen OK (1994) *Phys Rev B* 49(23):16223
54. Wu H, Zhang H, Cheng X, Cai L (2007) *Philos Mag* 87(23):3373. doi:[10.1080/14786430701286239](https://doi.org/10.1080/14786430701286239)
55. Zhuravlev Y, Kravchenko N, Obolonskaya O (2010) *Russ J Phys Chem B* 4(1):20. doi:[10.1134/s1990793110010045](https://doi.org/10.1134/s1990793110010045)
56. Paier J, Marsman M, Hummer K, Kresse G, Gerber IC, Angyan JG (2006) *J Chem Phys* 124(15):154709. doi:[10.1063/1.2187006](https://doi.org/10.1063/1.2187006)
57. Tasker PW (1979) *J Phys C* 12(22):4977
58. Claudine N (2000) *J Phys* 12(31):R367